Novel Sensing Algorithm for Linear Read-Out of Bimodal Waveguide Interferometric Biosensors

Bernat Bassols-Cornudella, Patricia Ramirez-Priego, Maria Soler, M.-Carmen Estévez, Heriberto J. Díaz Luis-Ravelo, Maria Cardenosa-Rubio, and Laura M. Lechuga, *Member, IEEE, Fellow, OSA*

***Abstract*—Biosensors employing photonics integrated circuits, and specifically those that rely on interferometric evanescent wave working principles, have outstanding performances due to the extreme sensitivity exhibited in one-step and direct assay, without the need of amplification. Within the interferometric configurations, the Bimodal Waveguide (BiMW) interferometric sensor stands out due to its demonstrated sensitivity for real-life applications and the simplicity of its design. To overcome the ambiguities that arise from the periodic nature of interferometric read-outs, a new all-optical modulation and the subsequent trigonometry-based algorithm have been proposed and applied to the BiMW biosensor. This new algorithm has been successfully employed for the selective identification and quantification of the external Spike (S) protein of the Severe Acute Respiratory Syndrome Coronavirus 2 (SARS-CoV-2). Our biosensing results from this simple, quick, and user-friendly method demonstrate high sensitivity and specificity and pave the way towards a point-of-care device for general use.**

***Index Terms*—Biosensors, integrated optics, silicon photonics, waveguide interferometry, coronavirus.**

I. Introduction

THE need for rapid, highly sensitive, inexpensive, and portable platforms for the real-time detection of low concentrations of analytes has increased in recent years and has been revealed of paramount importance during the COVID-19 pandemic. Portable biosensors able to be used at the point-of-care (POC) are the most effective means of early diagnostics regarding clinical and pharmaceutical analysis, medical diagnostics [1], [2], environmental monitoring [3], and many other industrial applications. In this rapidly increasing field, photonic biosensors based on evanescent wave detection have shown to be one of the best candidates for such POC devices given their extremely high sensitivity [4]–[6]. More specifically, those based on interferometric architectures have shown a remarkably good sensitivity; 10^{-7}–10^{-8} refractive index units (RIU) for bulk detection and in the order of few pg/mm^2 for surface sensing, while presenting clear advantages for label-free analyses [1], [3], [4].

Classical interferometric architectures such as the Mach-Zehnder (MZI) [7]–[10], or Young interferometers [11]–[13] are based on two-path schemes. In these devices, an initial light beam is split into a reference branch where the evanescent probing field remains intact and a sensing branch responsible for guiding the light beam through a sensing area. The properties of the light beam traveling through the sensing branch will be altered depending on the refractive index (RI) of the analysed solution. As a result, interference takes place after recombining both light beams, producing quantifiable variations on the resulting light intensity.

Alternatively, single-path configurations have been proposed to simplify fabrication processes, as well as to reduce costs and footprint [14], [15]. In these devices, two light modes of different order or polarization propagate through the same waveguide, where their respective evanescent fields are affected by the RI of the analysed solution simultaneously. The displacement between these modes results in an interferometric output, measurable either as a variation of the far-field pattern created at the sensor output and quantifiable by their relative phase variation or as an intensity deviation after recombining both waves into a single mode [16], [17]. This idea was first put into practice with optical fibres [18]–[22] and later applied to silicon photonics, resulting in the emergence of the Bimodal Waveguide (BiMW) interferometric biosensor [17], [23].

Interferometric biosensors can achieve very accurate and sensitive results at the expense of hindering the read-out response. The periodic (sinusoidal) nature of the output intensity with respect to phase variations raises a series of analytical difficulties when trying to evaluate the phase displacement, i.e., the evaluated parameter $\Delta\varphi$, such as sensitivity fading, fringe order, and direction ambiguities, as shown in Fig. 1.

In order to overcome these drawbacks and obtain an unambiguous read-out, a wide range of phase compensation and modulation techniques have been suggested. They are based on a variety of physical principles induced by electro and magneto-optical components [24]–[27], thermo-optical properties [28], or rely on the use of liquid crystals and photosensitive layers [29], [30]. Further research has also been carried out for the implementation of spectral interrogation

Manuscript received June 1, 2021; revised August 28, 2021; accepted September 30, 2021. Date of publication October 6, 2021; date of current version January 3, 2022. This work was supported by the H2020 Research and Innovation Programme of the European Commission (CONVAT project, H2020-SC1-PHE-CORONAVIRUS-2020) under Grant 101003544. The ICN2 was supported by the CERCA programme of the Generalitat de Catalunya and by the Severo Ochoa Centres of Excellence Program, funded by the AEI under Grand SEV-2017-0706. *(Corresponding author: Laura M. Lechuga.)*

The authors are with the Nanobiosensors and Bioanalytical Applications Group (NanoB2A), Catalan Institute of Nanoscience and Nanotechnology (ICN2), CSIC, CIBER-BBN and BIST, 08193 Barcelona, Spain (e-mail: bernat.bassols-cornudella20@imperial.ac.uk; patricia.ramirez@icn2.cat; maria.soler@icn2.cat; mcarmen.estevez@icn2.cat; heriberto.diazluis@gmail.com; maricruz.cardenosa@icn2.cat; laura.lechuga@icn2.cat).

Color versions of one or more figures in this article are available at https://doi.org/10.1109/JLT.2021.3118103.

Digital Object Identifier 10.1109/JLT.2021.3118103

This work is licensed under a Creative Commons Attribution-NonCommercial-NoDerivatives 4.0 License. For more information, see https://creativecommons.org/licenses/by-nc-nd/4.0/

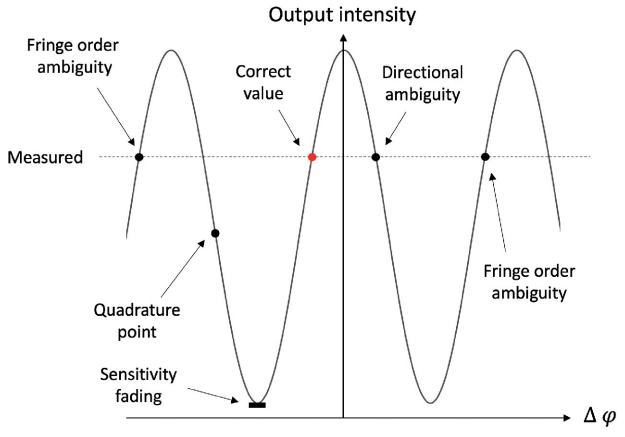

Fig. 1. Usual interferometric output ambiguities that hinder the quantification of the signal: sensitivity fading, directional ambiguities and fringe order ambiguities. The correct value to be measured is highlighted in red and the quadrature point, where sensitivity is maximized, is also shown.

techniques that have been successfully applied on slightly modified MZI versions [31]–[36]. However, the practical execution of these methods requires the addition of expensive and space-demanding equipment such as high precision spectrometers, narrowband tunable lasers, or an extensive modification of optimized fabrication protocols. Our group previously proposed an all-optical modulation technique together with an algorithm based on Fourier Series deconvolution for achieving a linear read-out of the MZI and the BiMW biosensor [37]–[39]. A simple implementation was feasible due to the use of commercial laser diodes under high-frequency intensity modulations, without the need to incorporate any extra apparatus.

Now we propose a novel and improved BiMW read-out algorithm based on simple trigonometric properties of the periodic read-out signal, which has been implemented using custom-made software. The proposed method uses an all-optical modulation technique as previously applied in [37], although slightly modified for employing the new algorithm, resulting in a faster, more sensitive, and user-friendly modulation technique with no additional costly equipment. We show the excellent performance of this new read-out algorithm with a biosensing proof-of-concept by detecting the external Spike (S) protein of the Severe Acute Respiratory Syndrome Coronavirus 2 (SARS-CoV-2). This new algorithm has been optimized for its use with the BiMW interferometric biosensor, although it could be extended to any other interferometric-based platform that allows a sinusoidal intensity-induced phase modulation such as the one presented below.

II. The BiMW Interferometric Biosensor

A. Sensor Working Principle

The BiMW biosensor working principle relies on the change of the properties of a monochromatic transverse electric (TE) polarized light beam [23]. The waveguide is a three-dimensional (2.5–3 μm width $\times$ 2–3 nm height $\times$ 3 cm length) rib waveguide made of a silicon dioxide (SiO2, RI $= 1.46 \pm 0.01$ RIU) cladding and a silicon nitride (Si3N4, RI $= 2.00 \pm 0.01$ RIU) core that allows the propagation of the fundamental and first TE modes, previously shown to be the most sensitive ones [38]. More specifically, as shown in Fig. 2, when light travels through the waveguide, it first encounters a single-mode section (150 nm thickness) in which the light solely propagates in its fundamental mode. This region is followed by a modal splitter, i.e., a rigorously engineered step junction that geometrically tolerates the appearance of the first mode. After this point, both modes propagate through the bimodal section (340 nm thickness) until the waveguide exit. In this bimodal section, a rectangular part of the upper cladding is removed to create the sensing area (centred with dimensions $=$ 50 μm width $\times$ 15 mm length). In general, as light travels through a waveguide, its physical properties are determined by the core and the top and bottom claddings refractive indexes. Therefore, any change in the materials will produce a variation of the light propagation properties. To be more precise, as both modes propagate along the bimodal section (see Fig. 2), their evanescent field, i.e., the electric field exponential tails that slightly penetrate into the claddings (see equation (3.53) in [40]), are altered by the corresponding RI of the material. When the two modes reach the sensing area, they are affected by the solution or the molecules attached to its surface. Any change to this external environment will imply a change on the top cladding RI, inducing a quantifiable variation to the properties of the probing light beam.

Once the propagating modes have crossed the device, they exit the waveguide such that, if projected on a screen, light expands vertically, forming a bright, straight line containing the interferometric output as shown in Fig. 2.

B. Experimental Setup and Output

The visible light travelling in the BiMW interferometric sensor was generated by a commercial laser diode (HL6545MG, $\lambda = 600$ nm, Thorlabs, Newton, New Jersey, USA) plugged in a miniature temperature-controlled Cooled Mount (LDM21, Thorlabs, Newton, New Jersey, USA) and kept at a constant temperature of 25.00 ± 0.01 °C. An aspheric lens (C240TMD-B, Thorlabs, Newton, New Jersey, USA) directed the emitted light towards the preferred direction as a collimated light beam. The light beam was then polarized in the TE direction by a free-space isolator (IO-3D-660-VLP, Thorlabs, Newton, New Jersey, USA) and focused on the waveguide entrance by a 40$\times$ optical objective (Olympus PLN 40$\times$ Objective, Edmund Optics, Barrington, New Jersey, USA). A total of 20 operative sensing bimodal waveguides are included in each sensor chip (3 cm long $\times$ 1 cm width), fabricated at wafer-scale in the cleanroom facilities of the Institute of Microelectronics of Barcelona (IMB-CNM-CSIC), as previously described [23]. The sensor chips were placed on a custom-made, temperature-controlled holder adjustable for the coupling of the light in the waveguide. A fluidic system ensures the continuous flow of a buffer solution over the sensor chip and the liquid sample injection to be analysed on the sensing area. The fluidic system includes a polydimethylsiloxane (PDMS) microfluidic cell with five channels (channel dimensions $=$ 1.25 mm wide $\times$ 500 μm height) that is hermetically sealed to the sensor chip; a syringe

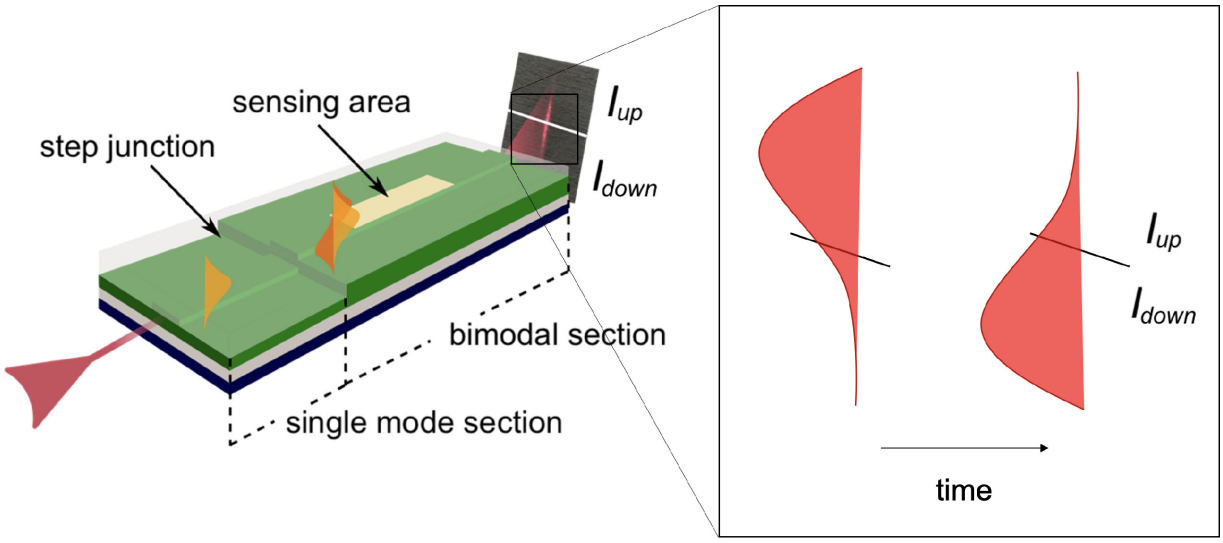

Fig. 2. BiMW sensor sketch showing the single mode propagating section, the bimodal section, the step junction, and the sensing area. Travelling light modes are simulated in orange for both sections, single and bimodal. As the laser beam, in red, exits the waveguide, it expands vertically when projected on a screen. Horizontally separated intensities I_{up} and I_{down} are recorded in real-time. When a sample is injected in the sensor, and under no laser intensity modulations, the light distribution output will shift up and down as shown in the magnified window.

pump (New Era, US) for the continuous flow of the running buffer solution (e.g., milli-Q water, phosphate-buffered saline, etc.); and a 6-port valve (CHEMINERT, VICI, USA) for the injection of the samples in the sensor. The light output was recorded by a horizontally split two-sectional photodetector (S4349, Hamamatsu, Japan). The received data was collected by an acquisition card (NI USB-6361, National Instruments, USA) and treated by a custom-made Python software. Due to the interferometric nature of the device, RI changes on the chip sensing area caused the vertical output line to shift up and down. This oscillatory movement was recorded and converted into a quantifiable signal able to measure any RI changes in the sensing area. Having a two-sectional photodetector provided real-time values for the intensities I_{up} and I_{down} shown in Fig. 2, such that without any external tunning of the laser intensity, i.e. under a non-modulating regime, we could define the sensitivity parameter, S_R [23], [37]–[39], [41], as follows,

$$S_R = \frac{I_{up} - I_{down}}{I_{up} + I_{down}} = A + B\cos\varphi, \tag{1}$$

where φ is the light phase. Changes like the flow of a new substance on the sensing area or the binding of biomolecules resulted in variations on the light propagation characteristics and, therefore, on its phase φ and the signal S_R. Hence, Eq. (1) shows that as time goes by and no changes on the sensing area occur, the sensor output will remain a continuous straight line, and φ will not be altered. In other words, if a solution of the same RI as the buffer flows through the sensing area (e.g., milli-Q water while also running milli-Q water), no changes in the S_R will be observed. However, the flow of a different refractive index solution (e.g., hydrochloric acid (HCl) 0.1 M, $\Delta_n = (8.21 \pm 0.01) \times 10^{-4}$ RIU) generates the oscillations on the output as φ varies, changing the S_R sinusoidally. This behaviour is shown in Fig. 3, where the S_R signal sinusoidally oscillates if and only if a change in φ occurs.

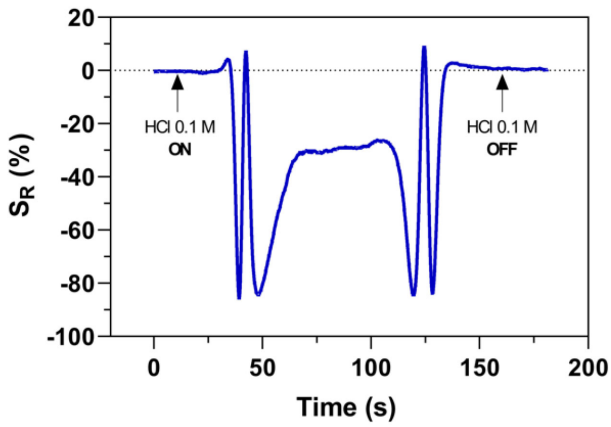

Fig. 3. Recorded SR signal during the detection of HCl 0.1 M injection under milli-Q water constant flow, with a RI change $\Delta n = (8.21 \pm 0.01) \times 10^{-4}$ RIU.

C. Phase Retrieval Techniques. A New Algorithm

A phase retrieval process must be carried out in order to obtain the temporal evolution of the phase φ. This is only possible in relative terms by computing the phase difference $\Delta\varphi$ between that of the initial solution and the introduced one. Then, $\Delta\varphi$ is compared to a set of calibration values from which the solution RI is finally acquired. However, the non-bijective periodic nature of the S_R signal and its resulting phase fringe and direction ambiguities as well as a potential sensitivity fading, hinder this process and make it much more complex than desired. Previous methods involved counting fringes and periods provided the computed signal is a 2π-periodic function under static intensity or applying an experimentally restrictive sinusoidal intensity modulation followed by an algorithm based on Fast Fourier transforms and the Bessel functions of the first kind of order 2 and 3 [37]–[39]. To solve these drawbacks, a new

all-optical modulation algorithm based on simple trigonometric relationships was designed and implemented to easily retrieve the pursued phase difference, $\Delta\varphi$.

As presented in [39] and [42], we can induce a new term in the S_R expression by sinusoidally modulating the intensity, such that Eq. (1) is modified to obtain Eq. (2):

$$S_R = A + B\cos(\Delta\varphi + \varphi_0 + \mu\sin\omega t), \tag{2}$$

where t is the time, ω is the modulating frequency, and μ is the modulation depth, altogether constituting the modulating term, $\mu\sin\omega t$. Note that $\Delta\varphi = \varphi - \varphi_0$, being φ_0 the phase corresponding to the previously mentioned running buffer. Notice that neither A nor B constants are the same as those previously defined in Eq. (1).

The first step in the algorithm consists in removing the offset A from the signal. This can be done assuming $\mu \geq \pi$, which allows the cosine to fill all its image space, from -1 to 1 regardless of φ_0 and $\Delta\varphi$, ensuring the S_R to be well defined and surjectively fill the interval $[A - B, A + B]$. Thus, the new centered signal presented in Eq. (3) will be considered from now on, specifically:

$$\begin{aligned} S'_R &= S_R - \frac{\max S_R + \min S_R}{2} \\ &= B\cos(\Delta\varphi + \varphi_0 + \mu\sin\omega t), \end{aligned} \tag{3}$$

for which, due to an abuse of notation, we shall drop the prime superindex. Let us consider the beginning of a measurement, in which the running buffer is kept constant such that $\Delta\varphi = 0$. In this case, the recorded S_R signal from Eq. (3) reaches its maximum B at a time t_1, if $\varphi_0 + \mu\sin\omega_{t_1} = 2\pi k_1$, for $k_1 \in \mathbb{Z}$, and becomes 0 at a time t_0 if $\varphi_0 + \mu\sin\omega t_0 = \pi/2 + \pi k_0$, for $k_0 \in \mathbb{Z}$. Therefore, constantly modulating under the same sinusoidal signal we can determine times t_0 and t_1 such that if we compute the S_R at these times, we obtain Eq. (4) and Eq. (5):

$$\begin{aligned} S_{R,t_0} &= B\cos(\Delta\varphi + \varphi_0 + \mu\sin\omega t_0) \\ &= B\cos\left(\Delta\varphi + \frac{\pi}{2} + \pi k_0\right) \\ &= -B\sin(\Delta\varphi + \pi k_0) \\ &= (-1)^{k_0+1} B\sin\Delta\varphi, \end{aligned} \tag{4}$$

$$\begin{aligned} S_{R,t_1} &= B\cos(\Delta\varphi + \varphi_0 + \mu\sin\omega t_1) \\ &= B\cos(\Delta\varphi + 2\pi k_1) \\ &= B\cos\Delta\varphi. \end{aligned} \tag{5}$$

The phase difference information can now be directly retrieved dividing these expressions to get Eq. (6) and finally Eq. (7):

$$\begin{aligned} \frac{S_{R,t_0}}{S_{R,t_1}} &= \frac{(-1)^{k_0+1} B\sin\Delta\varphi}{B\cos\Delta\varphi} \\ &= (-1)^{k_0+1}\tan\Delta\varphi, \end{aligned} \tag{6}$$

$$\Delta\varphi = (-1)^{k_0+1}\arctan\frac{S_{R,t_0}}{S_{R,t_1}}, \tag{7}$$

since the arctangent function can be easily unwrapped computationally [39]. Note that the sign of the phase shift will always be known before any measurement as it is possible if the RI increases with respect to the running buffer and negative if it decreases. Thus, the term $(-1)^{k_0+1}$ shall not be taken as an inconvenience. Furthermore, this algorithm is applicable to any type of sinusoidal signal in which a time-dependent phase variation behaving like the modulating term presented above can be induced.

To modulate the laser diode emission and apply the algorithm presented, a custom-made Python application was developed. Specifically, the laser intensity was sinusoidally modulated from 100 to 200 mA at a frequency of 10 Hz. Such intensity changes induced a linear displacement of the central wavelength emitted by the laser diode, resulting in the addition of the modulating term $\mu\sin\omega t$. It must be noted that for each probed laser intensity, the emitted wavelength distribution is very narrowly supported near its mean, covering less than 0.5 nm around the centre, while being displaced almost 10 nm for the considered intensity modulation. At the same time, these characteristics are not dependant on the modulating frequency and do not induce a perceivable noise on the system.

The only restriction the proposed algorithm imposes is the need to have a value of $\mu \geq \pi$. This has been proven to be true as long as the intensity modulating amplitude is higher than 80 mA. To ensure a correct behaviour, it was decided to modulate from 100 to 200 mA while remaining in the recommended intensity range of the laser diode and not forcing it to extreme values. Moreover, the measuring times t_0 and t_1 used in the presented phase retrieval method are not unique in most cases. Depending on the S_R obtained, more than one value for t_0 or t_1 can be found, thus allowing us to apply the algorithm to all possible pair combinations and consider the one showing a lower noise, overall increasing the biosensor sensitivity with respect to previously employed phase retrieval methods.

If compared to the previous technique proposed in [39], there are three key differences to be outlined. First, our new algorithm allows for the use of a larger number of sensor chips since the previous method requires a strictly fixed value of $\mu = 1.2\pi$. Although usually achievable, slight fabrication tolerances may make this unfeasible for certain sensor chips. Second, the modulating frequency of 10 Hz ensures at least the same number of phase retrievals per second and can be increased accordingly with compounds inducing strong RI which are used during the experiments. Finally, the algorithm takes place in the time domain instead of the frequency domain, which eases its technical understanding by multidisciplinary users. Hence, the proposed algorithm is faster, simpler, and more user friendly, altogether opening the way to be implemented in POC biosensor platforms.

D. Bulk Sensing Evaluation

In order to evaluate the bulk refractive index sensitivity of the BiMW interferometric biosensor under the discussed algorithm, five different HCl solutions (0.025, 0.05, 0.1, 0.25, and 0.5 M), whose respective refractive indexes were measured with a digital refractometer (Rudolph Research Analytical, USA), were sequentially injected through the microfluidic system into the sensing area, while milli-Q water was used as running buffer at a constant flow rate of 20 μl/min.

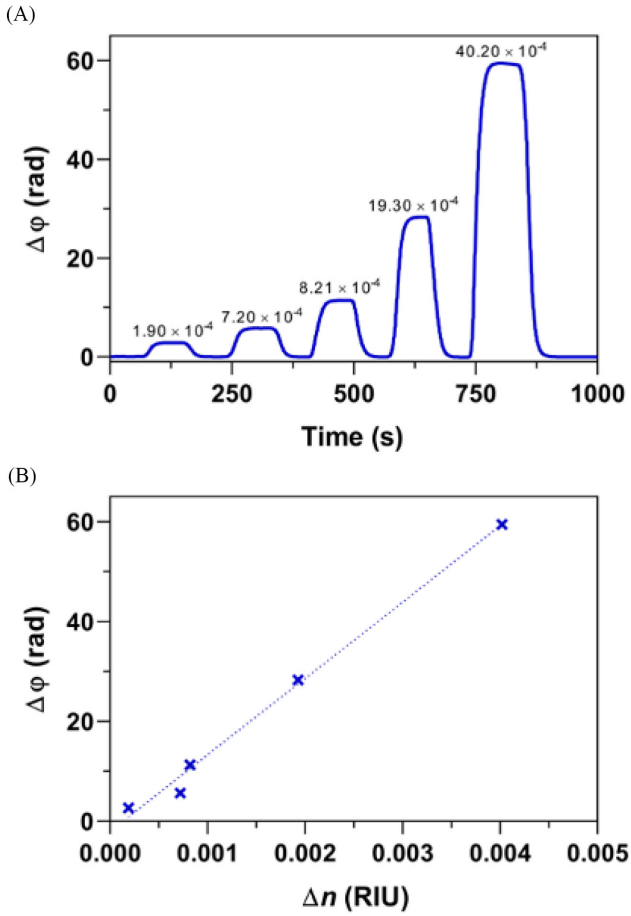

Fig. 4. (A) Real-time computed phase difference during HCl calibration procedure with five different concentrations. The RI difference with respect to milli-Q, Δn is given in RIU with an error of 0.01×10^{-4}. (B) Calibration curve with its corresponding linear fit, $r^2 = 0.9998$, $LOD = (3.21 \pm 0.01) \times 10^{-7}$ RIU. Plotted points correspond to the average of six measurements with a standard deviation of approximately 0.01 that cannot be appreciated in the plot.

The new phase retrieval method was applied and the respective phase differences of each injection, $\Delta\varphi$, were computed. Figs. 4(A) and (B) show the variation of the phase depending on the HCl concentration and the calibration curve obtained by plotting the phase difference for each HCl solution as a function of the refractive index change. The limit of detection (LOD) of the sensor is defined as the minimum variation of RI that produces a signal at least three times higher than the detectable noise of the system. It is computed as $LOD = 3\sigma/S_{bulk}$, where σ is the standard deviation of the retrieved phase, which results from the propagated error of the mean of the standard deviation after five experiments that run for 200 seconds with milli-Q water, and S_{bulk} is the slope of the linear regression in Fig. 4(B). Evaluations of the same sensor chip and different sensor chips showed consistent results of a LOD between 2 and 5×10^{-7} RIU. These values demonstrate the validity of the newly proposed algorithm as the results are identical to those obtained employing previous techniques [37]. In fact, we did not expect the algorithm to provide different phase variation values from the ones obtained using other methods since the evaluated parameter was the same, $\Delta\varphi$. On the other hand, this method was able to follow real-time large and small refractive index variations happening on the sensing area with more precision, as well as lower noise ($\sigma = 0.00184$ rd) as compared with previous methods (see [43]).

E. Biosensing Evaluation

To fully demonstrate the new all-optical modulation capabilities for biosensing purposes, the rapid and direct detection of a specific structural protein of the novel Severe Acute Respiratory Syndrome Coronavirus 2 (SARS-CoV-2) was assessed. Among all the SARS-CoV-2 viral antigens, the external spike (S) protein is a trimetric glycoprotein that plays an essential role in the infection, mediating the binding of the viral particles to host surface cellular receptors. The S protein comprises two functional subunits: S1 subunit that contains the receptor-binding domain, which directly binds to the host cell receptor angiotensin-converting enzyme 2, and S2 subunit, which is responsible for the membrane fusion. As a proof-of-concept, S1 subunit was selected as the target analyte to be recognized by its specific antibody previously immobilized on the sensor chip surface.

The BiMW sensor chip was first functionalized with triethoxysilane polyethylene glycol carboxylic acid (silane-PEG-COOH 600 Da; Nanocs, New York, USA), following our protocol previously detailed in [44]. The silanized sensor chip was directly placed into the experimental setup for further in-situ covalent binding of the antibodies. Carboxylic groups provided by the silane-PEG-COOH were activated employing the well-known N-(3-dimethylaminopropyl)-N′-ethylcarbodiimide hydrochloride (EDC)/N-hydroxysulfosuccinimide (sulfo-NHS) chemistry, highly reactive to primary amine groups accessible in the lysine residues of the antibodies. A solution with 0.2 M EDC/0.05 M sulfo-NHS in MES buffer (2-(N-morpholino)ethanesulfonic acid 0.1 M, pH 5.5) was flowed over the sensor surface. Next, a solution with 50 μ g/mL of the specific chimeric monoclonal antibody against Spike protein (anti-S chAb, 40150-D001, Sino Biological Inc., China) in acetate buffer (10 mM, pH 5.5) was injected. After antibody binding, a stable covalent amide bond was formed. The remaining activated carboxyl groups were blocked with ethanolamine (1 M, pH 8.5) for 2 min. All steps of the immobilization of the anti-S chAb were monitored in real-time with the new algorithm (see Fig. 5 A). Milli-Q water was used as the running buffer during the immobilization step and was then switched to PBST buffer (phosphate buffer saline (PBS 10 mM) with 0.05% Tween 20, pH 7.4) for the detection of S1 subunit protein.

Different S1 concentrations ranging from 50 to 1000 ng/mL were flowed over the sensor surface. As shown in Fig. 5(B), the biosensor response in real-time exhibits a correlation between the analysed concentration and the response. Furthermore, the injection of a control protein (1 μg/mL C-reactive protein, BBI Solutions, U.K.) confirms that the antibody exclusively recognized the specific SARS-CoV-2 S1 subunit protein with no cross-reactivity. The obtained calibration curve shows a linear concentration-dependent response ($r^2 = 0.98$) resulting in a LOD of 6.45 ng/mL. These results demonstrate that we could develop an effective biosensor with the BiMW sensor and

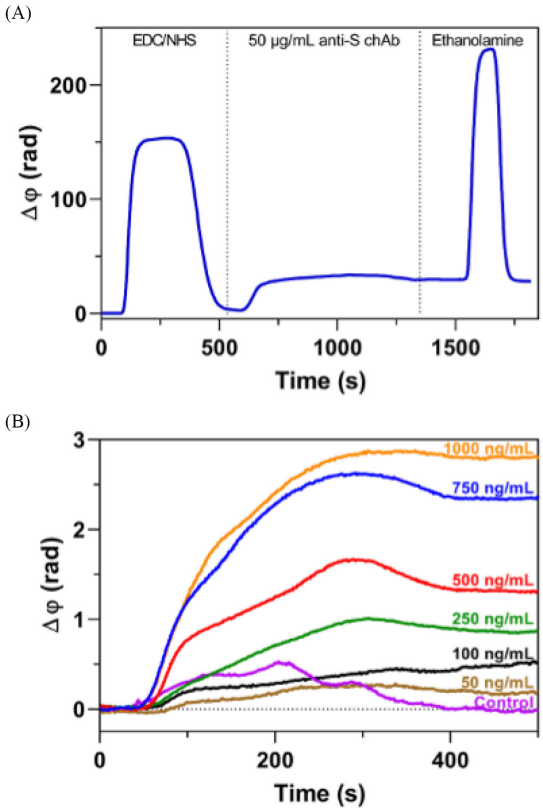

Fig. 5. Real-time sensorgrams showing (A) the immobilization of 50 μg/mL anti-S chAb, and (B) the following detection of different S1 subunit concentrations (50 - 1000 ng/mL) in comparison to the control protein (1000 ng/mL CRP).

the new algorithm to identify and quantify SARS-CoV-2 spike protein in less than 10 min with high sensitivity and specificity.

III. Conclusion

A new algorithm has been implemented with a custom-made software application in order to retrieve the phase difference from the real-time recorded data. This method based on simple trigonometry was proven to provide the same results as previously employed techniques while also reducing the sensor noise as well as the time and expertise needed to employ the biosensor, making the BiMW platform more user-friendly. In addition, the algorithm can be easily applied to any interferometric device whose output signal behaves similarly to the S_R described, without increasing the intricacy of design nor fabrication protocols. The aforementioned advances have pushed the BiMW interferometric biosensor much closer to a user-friendly competitive tool, increasing its potential to be assembled into a truly POC device.

Acknowledgement

This work was supported by the H2020 Research and Innovation Programme of the European Commission (CONVAT project, H2020-SC1-PHE- CORONAVIRUS-2020) under Grant 101003544. The ICN2 was supported by the CERCA programme of the Generalitat de Catalunya and by the Severo Ochoa Centres of Excellence Program, funded by the AEI under Grand SEV- 2017-0706. We are very grateful to EPI Industries (Barcelona, Spain) for its kind donation supporting our research on COVID-19.

References

[1] C. S. Huertas, D. Fariña, and L. M. Lechuga, "Direct and label-free quantification of Micro-RNA-181a at attomolar level in complex media using a nanophotonic biosensor," *ACS Sensors*, vol. 1, no. 6, pp. 748–756, 2016.
[2] M. Soler, C. S. Huertas, and L. M. Lechuga, "Label-free plasmonic biosensors for point-of-care diagnostics: A review," *Expert Rev. Mol. Diagn.*, vol. 19, no. 1, pp. 71–81, 2019.
[3] B. Chocarro-Ruiz *et al.*, "Interferometric nanoimmunosensor for label-free and real-time monitoring of Irgarol 1051 in seawater," *Biosensors Bioelectron.*, vol. 117, pp. 47–52, 2018.
[4] P. Kozma, F. Kehl, E. Ehrentreich-Förster, C. Stamm, and F. F. Bier, "Integrated planar optical waveguide interferometer biosensors: A comparative review," *Biosensors Bioelectron.*, vol. 58, pp. 287–307, 2014.
[5] D. P. Campbell, "Interferometric biosensors," in *Princ. of Bacterial Detection: Biosensors, Recognit. Receptors and Microsystems*. New York, NY, USA: Springer, 2008, pp. 169–211.
[6] A. Brandenburg, R. Krauter, C. Künzel, M. Stefan, and H. Schulte, "Interferometric sensor for detection of surface-bound bioreactions," *Appl. Opt.*, vol. 39, no. 34, pp. 6396–6405, 2000.
[7] R. G. Heideman, R. P. Kooyman, and J. Greve, "Performance of a highly sensitive optical waveguide Mach-Zehnder interferometer immunosensor," *Sensors Actuators: B. Chem.*, vol. 10, no. 3, pp. 209–217, 1993.
[8] F. Prieto *et al.*, "An integrated optical interferometric nanodevice based on silicon technology for biosensor applications," *Nanotechnol.*, vol. 14, pp. 907–912, 2003.
[9] B. H. Schneider, J. G. Edwards, and N. F. Hartman, "Hartman interferometer: Versatile integrated optic sensor for label- free, real-time quantification of nucleic acids, proteins, and pathogens," *Clin. Chem.*, vol. 43, no. 9, pp. 1757–1763, 1997.
[10] B. H. Schneider, E. L. Dickinson, M. D. Vach, J. V. Hoijer, and L. V. Howard, "Highly sensitive optical chip immunoassays in human serum," *Biosensors Bioelectron.*, vol. 15, no. 1-2, pp. 13–22, 2000.
[11] A. Brandenburg and R. Henninger, "Integrated optical young interferometer," *Appl. Opt.*, vol. 33, no. 25, pp. 5941–5947, 1994.
[12] A. Ymeti, J. S. Kanger, R. Wijn, P. V. Lambeck, and J. Greve, "Development of a multichannel integrated interferometer immunosensor," *Sensors Actuators, B: Chem.*, vol. 83, no. 1-3, pp. 1–7, 2002.
[13] K. Schmitt, B. Schirmer, C. Hoffmann, A. Brandenburg, and P. Meyrueis, "Interferometric biosensor based on planar optical waveguide sensor chips for label-free detection of surface bound bioreactions," *Biosensors Bioelectron.*, vol. 22, no. 11, pp. 2591–2597, 2007.
[14] I. Barth, D. Conteduca, C. Reardon, S. Johnson, and T. F. Krauss, "Common-path interferometric label-free protein sensing with resonant dielectric nanostructures," *Light: Sci. Appl.*, vol. 9, no. 96, 2020.
[15] R. Magnusson, K. J. Lee, and D. Wawro, "Guided-mode resonance biosensors employing phase detection," in *Diffractive Opt. Micro-Opt.*, 2004, Paper DTuC 2.
[16] K. A. Murphy, M. S. Miller, A. M. Vengsarkar, and R. O. Claus, "Elliptical-core two-mode optical-fiber sensor implementation methods," *J. Lightw. Technol.*, vol. 8, no. 11, pp. 1688–1696, 1990.
[17] C. D. Horna, K. E. Zinoviev, and L. M. Lechuga, "Interferometer and sensor based on bimodal optical waveguides, and detection method," U.S. Patent no. 8279445-B2, 2007.
[18] M. Spajer, "Linear phase detection for a bimodal fiber sensor," *Opt. Lett.*, vol. 13, no. 3, p. 239, 1988.
[19] A. M. Vengsarkar, W. C. Michie, B. Culshaw, L. Jankovic, and R. O. Claus, "Fiber-optic dual-technique sensor for simultaneous measurement of strain and temperature," *J. Lightw. Technol.*, vol. 12, no. 1, pp. 170–177, 1994.
[20] J. Canning and A. L. G. Carter, "Modal interferometer for in situ measurements of induced core index change in optical fibers," *Opt. Lett.*, vol. 22, no. 8, p. 561, 1997.
[21] R. X. Gao, Q. Wang, F. Zhao, B. Meng, and S. L. Qu, "Optimal design and fabrication of SMS fiber temperature sensor for liquid," *Opt. Commun.*, vol. 283, no. 16, pp. 3149–3152, 2010.
[22] R. Poozesh *et al.*, "Experimental study and simulation of modular interference in two-mode fiber," *Opt. Spectrosc. (English Transl. Optika i Spektroskopiya)*, vol. 111, no. 2, pp. 284–286, 2011.

[23] A. B. González-Guerrero, C. Domínguez, K. E. Zinoviev, and L. M. Lechuga, "Integrated bimodal waveguide interferometric biosensor for label-free analysis," *J. Lightw. Technol.*, vol. 29, no. 13, pp. 1926–1930, 2011.
[24] U. Minoni, E. Sardini, E. Gelmini, F. Docchio, and D. Marioli, "A high-frequency sinusoidal phase-modulation interferometer using an electro-optic modulator: Development and evaluation," *Rev. Sci. Instruments*, vol. 62, no. 11, pp. 2579–2583, 1991.
[25] B. Maisenhölder, H. P. Zappe, R. E. Kunz, P. Riel, M. Moser, and J. Edlinger, "A GaAs/AlGaAs-based refractometer platform for integrated optical sensing applications," *Sensors Actuators, B: Chem.*, vol. 39, no. 1-3, pp. 324–329, 1997.
[26] P. V. Lambeck, "Remote opto-chemical sensing with extreme sensitivity: Design, fabrication and performance of a pigtailed integrated optical phase-modulated mach-zehnder interferometer system," *Sensors Actuators, B: Chem.*, vol. 61, no. 1, pp. 100–127, 1999.
[27] B. Sepúlveda, G. Armelles, and L. Lechuga, "Magneto-optical phase modulation in integrated Mach-Zehnder interferometric sensors," *Sensors Actuators A: Phys.*, vol. 134, no. 2, pp. 339–347, 2007.
[28] V. M. N. Passaro, F. Magno, and A. V. Tsarev, "Investigation of thermo-optic effect and multi-reflector tunable filter/multiplexer in SOI waveguides," *Opt. Exp.*, vol. 13, no. 9, p. 3429, 2005.
[29] A. Hamori, K. Cottier, and R. Horvath, "Grating coupled interferometry for optical sensing," *Appl. Phys. B*, vol. 97, no. 1, pp. 5–8, 2009.
[30] A. Dér, S. Valkai, A. Mathesz, I. Andó, E. K. Wolff, and P. Ormos, "Protein-based all-optical sensor device," *Sensors Actuators B: Chem.*, vol. 151, no. 1, pp. 26–29, 2010.
[31] T. Pinheiro-Ortega, E. Silvestre, P. Andrés, B. Maes, and P. Bienstman, "Design of bimodal PCFs for interferometric gas sensors with high sensitivity," *IEEE Sensors J.*, vol. 10, no. 7, pp. 1180–1184, Jul. 2010.
[32] R. Halir, L. Vivien, X. Le Roux, D.-X. Xu, and P. Cheben, "Direct and sensitive phase readout for integrated waveguide sensors," *IEEE Photon. J.*, vol. 5, no. 4, pp. 6800 906–6800906, Aug. 2013.
[33] M. Kitsara, K. Misiakos, I. Raptis, and E. Makarona, "Integrated optical frequency-resolved Mach-Zehnder interferometers for label-free affinity sensing," *Opt. Exp.*, vol. 18, no. 8, pp. 8193–8206, 2010.
[34] M. L. Notte and V. M. Passaro, "Ultra high sensitivity chemical photonic sensing by Mach-Zehnder interferometer enhanced vernier-effect," *Sensors Actuators, B: Chem.*, vol. 176, pp. 994–1007, 2013.
[35] T. Hutter, S. R. Elliott, and S. Ruschin, "Dynamic range enhancement and phase-ambiguity elimination in wavelength-interrogated interferometric sensor," *Sensors Actuators, B: Chem.*, vol. 178, pp. 593–597, 2013.
[36] K. Misiakos *et al.*, "Broad-band Mach-Zehnder interferometers as high performance refractive index sensors: Theory and monolithic implementation," *Opt. Exp.*, vol. 22, no. 8, pp. 8856–8870, 2014.
[37] S. Dante, D. Duval, D. Fariña, A. B. González-Guerrero, and L. M. Lechuga, "Linear readout of integrated interferometric biosensors using a periodic wavelength modulation," *Laser Photon. Rev.*, vol. 9, no. 2, pp. 248–255, 2015.
[38] D. Duval *et al.*, "Nanophotonic lab-on-a-chip platforms including novel bimodal interferometers, microfluidics and grating couplers," *Lab a Chip*, vol. 12, no. 11, pp. 1987–1994, 2012.
[39] S. Dante, D. Duval, B. Sepúlveda, A. B. González-Guerrero, J. R. Sendra, and L. M. Lechuga, "All-optical phase modulation for integrated interferometric biosensors," *Opt. Exp.*, vol. 20, no. 7, pp. 7195–7205, 2012.
[40] G. Lifante, *Integrated Photonics: Fundamentals*. Chichester, U.K.: Wiley, Ltd, 2003.
[41] D. G. García, D. Jiménez, J. R. Sendra, and L. M. Lechuga, "Lab-on-a-chip integration of the bimodal waveguide nanointerferometric biosensor," Ph.D. dissertation, Universitat Autònoma de Barcelona: Barcelona, Spain, 2018.
[42] O. Sasaki and H. Okazaki, "Sinusoidal phase modulating interferometry for surface profile measurement," *Appl. Opt.*, vol. 25, no. 18, pp. 3137–3140, 1986.
[43] P. Ramirez-Priego, M.-C. Estévez, H. J. Díaz-Luisravelo, J. J. Manclús, Á. Montoya, and L. M. Lechuga, "Real-time monitoring of fenitrothion in water samples using a silicon nanophotonic biosensor," *Analytica Chimica Acta*, vol. 1152, 2021, Art. no. 338276.
[44] J. Maldonado, M. C. Estévez, A. Fernández-Gavela, J. J. González-López, A. B. González-Guerrero, and L. M. Lechuga, "Label-free detection of nosocomial bacteria using a nanophotonic interferometric biosensor," *Analyst*, vol. 145, pp. 497–506, 2020.

Bernat Bassols-Cornudella was born in Barcelona, Spain, in 1997. He received the B.Sc. degree in mathematics and the B.Sc. degree in physics from the Autonomous University of Barcelona, Bellaterra, Spain, in 2020, and the M.Sc. degree in applied mathematics from Imperial College London, London, U.K., in 2021, where he began his studies of random processes. He is currently working toward the Ph.D. degree in mathematics of random systems in a joint CDT Program between Imperial College London and the University of Oxford, U.K. In 2019, he joined Nanobiosensors and Bioanalytical Applications Group (NanoB2A), where he specialised in integrated photonics and highly sensitive optical biosensors, focusing on their mathematical modeling and signal processing algorithms. His main research focuses on the birth of chaos in random dynamical systems and their application to biological and ecological processes.

Patricia Ramirez-Priego was born in Vilafranca del Penedès, Barcelona, Spain, in 1993. She received the B.Sc. degree in biotechnology and the M.Sc. degree in omics data analysis from the University of Vic - Central University of Catalonia, Spain, in 2015 and 2016, respectively, and the Ph.D. degree in biotechnology from the Autonomous University of Barcelona, Bellaterra, Spain, in 2021, focused on the development of a low-cost point-of-care test for active Tuberculosis detection in human urine samples using a nanophotonic platform. Since 2015, she has been with the Nanobiosensors and Bioanalytical Applications Group (NanoB2A), Catalan Institute of Nanoscience and Nanotechnology (ICN2), where she is currently a Postdoctoral Researcher. Her main research interests include the development of silicon photonic biosensors, mainly focusing on their biofunctionalization and their final validation with the evaluation of real samples to demonstrate their potential in multiple applications ranging from biomedical applications to environmental monitoring.

Maria Soler was born in 1987 in Valencia, Spain. She received the Degree in chemistry from the University of Valencia, Valencia, Spain, in 2010 and the Ph.D. degree in biochemistry, molecular biology, and biomedicine from the Autonomous University of Barcelona, Bellaterra, Spain, in 2015, with international honor mentions. In 2011, she joined the Laboratory of Prof. Laura M. Lechuga with the Catalan Institute of Nanoscience and Nanotechnology (ICN2), Barcelona, Spain, for her master and doctorate studies. After a 3-year postdoctoral stage with the Ecole Polytechnique Federale de Lausanne, EPFL, Switzerland, since 2018, she is a Senior Researcher of the Nanobiosensors and Bioanalytical Applications Group (NanoB2A), ICN2. To date, she has authored or coauthored about 20 peer-reviewed articles in top-ranked journals, with more than 800 citations. Her research interests include the design and development of novel nanophotonic biosensors for biomedical applications, with a special focus in sensor biofunctionalization methods and technology validation for point-of-care clinical diagnostics and novel immunoengineering therapeutic studies. She has also been invited as keynote and plenary speaker in international conferences and actively contributes to scientific dissemination in outreach events and publications.

M.-Carmen Estévez was born in Barcelona, Spain. She received the Bachelor of Chemistry degree from the University of Barcelona, Spain, in 1998 and the M.Sc. and Ph.D. degrees in chemistry in 1999 and 2005, respectively, focused on the development of immunochemical techniques for environmental monitoring. She got a Postdoctoral Fellowship from the Government of Catalonia (Beatriu Pinós Grant) to perform a stay at the University of Florida (Dept. Chemistry, UF) between 2006 and 2008. She focused on nanobiotechnology applied to in-vitro diagnostics, through the production and application of fluorescent nanoparticles for bioanalysis. In 2009, she joined the Nanobiosensors and Bioanalytical Applications Group, Institut Català de Nanociència i Nanotecnologia (ICN2) and CSIC, Barcelona, Spain, as a Senior Researcher, where she focused on surface biofunctionalization and clinical diagnostics applications of label-free optical biosensors. She has coauthored more than 40 papers in leading journals in nanotechnology, analytical chemistry, biosensors and optics. She is an Active Reviewer in ACS, Elsevier, RSC, and Wiley journals. Her main research interests include plasmonic and silicon photonics sensors, their integration in compact prototypes and the development of biosensor based applications to demonstrate their potential for real clinical, industrial, and/or environmental applications, aiming at transferring them to decentralized settings.

Heriberto J. Díaz Luis-Ravelo was born in Santa Cruz de Tenerife, Spain, in 1988. He received the B.S. degree in telecommunications engineer, specialized in electronic systems, from Las Palmas de Gran Canaria University, in 2015 and the M.S. degree in telecommunications engineer from Las Palmas de Gran Canaria University, in 2017. He joined the Nanobiosensors and Bioanalytical Applications Group (NanoB2A), Catalan Institute of Nanoscience and Nanotechnology (ICN2), Barcelona, Spain, as a Research Engineer from 2017 to 2021. He worked in nanoplasmonic and bimodal waveguide interferometric biosensors, in which he worked on the development to control and monitor biosensors working on both hardware and software. Since 2021, he has been a Lead Software Engineer with QUSIDE Technology, Barcelona, Spain. He is working on the development to control and monitor the quantum random number generator (QRNG).

Mari Cardenosa-Rubio is currently a PROBIST Postdoctoral Fellow under the Marie Skłodowska-Curie Agreement No. 754510 with the Catalan Institute of Nanoscience and Nanotechnology, Barcelona, Spain. She did her undergraduate studies in biotechnology with the University of Salamanca, Salamanca, Spain. After that, she moved to Belgium and France to pursue the Erasmus Mundus Master in nanosciences and nanotechnology. Then, she got a fellowship from La Caixa to pursue post-graduate studies in North America. This fellowship allowed her to carry out her Ph.D. in chemistry with the University of Michigan, Ann Arbor, MI, USA. During this stage, she worked in silicon photonic microring resonators for the detection of noncoding RNAs and polyphosphates in complex matrices. In the NanoB2A, her current work is based on the development of protocols for the multiplex detection of biomarkers in clinical settings using the silicon bimodal waveguides.

Laura M. Lechuga is currently a Full Professor with Spanish National Research Council (CSIC) and the Head of the Nanobiosensors and Bioanalytical Applications Group, Catalan Institute of Nanoscience and Nanotechnology (ICN2), Barcelona, Spain and with the Networking Biomedical Research Center (CIBER-BBN). The principal focus of her research is the development of novel nanobiosensor devices based on nanoplasmonics and silicon-based photonics principles for point-of-care diagnostics. She has been at the forefront of the Photonic Biosensor area during more than eighteen years, making key contributions and opening new horizons in this field. She has authored or coauthored more than 260 articles, book chapters and proceedings, has eight families of patents, and has presented her work worldwide in more than 365 invited talks. Her research activities have encompassed from fundamental research to the technological operation of complete sensing platforms, including the technological transfer into products of social applicability. Her Group is considered as a world reference in this field. She has co-founded two spin-offs companies. The quality of her research has been recognised by prestigious prizes and awards, as the Physics, Innovation and Technology Prize from the Spanish Royal Physics Society (RSEF) and BBVA Foundation (2016), the Ada Byron Prize (2020), the King Jaume I Award in New Technologies and the Spanish National Research Prize in Tech Transfer in 2020 (the two last ones are the most prestigious research prizes in Spain), and the Burdinola Research Award in 2021. In 2020, during the COVID-19 pandemic, she has been included in the Expert Scientific Panel advising the Ministry of Science and Innovation and the Spanish Government in the management of the pandemic. She is a Fellow of OSA.